EVALUATION OF ANALYTICAL AEROACOUSTIC MODELS FOR A LOW-SPEED AXIAL VENTILATION SYSTEM

Marlène SANJOSE[1], Miguel PESTANA[2],
Stéphane MOREAU[1], Patrice CAULE[3]

[1] *Université de Sherbrooke, Mechanical Engineering,*
2500 blvd de l'Université, Sherbrooke QC J1K2R1, Canada

[2] *Université de Lyon, LMFA, École Centrale de Lyon*
36, avenue Guy de Collongue, 69134 Écully cedex, France

[3] *Safran Ventilation Systems*
10, place Marcel Dassault, 31702 Blagnac, France

SUMMARY

Several analytical aeroacoustic models are applied for a compact ducted ventilation system with high rotational speed with uniformly distributed blades and vanes. RANS simulations are performed at several mass-flow rates and provide the parameters to calibrate the noise sources for the rotor and stator acoustic models. Several blade response and acoustic propagation models have been evaluated. Due to the limited numbers of blades and vanes, the cascade effects are shown to be negligible. The propagation assuming infinite duct allows capturing the cut-off frequencies but does not modify the global spectral shape of the results. The flow parameters which define the strength of interaction mechanisms are the crucial parameters for the acoustic results. For tonal noise, the rotor wake deficit at the stator leading-edge can be modeled using a Gaussian shape evolution model fitted from RANS extracted data. This model provides a satisfactory estimation and a good trend for flow rates above design but is not robust for the lowest flow rates investigated. The third blade passing frequency is overestimated by 8 dB with the present wake evolution model and with an isolated airfoil response with in-duct propagation. For broadband noise, turbulence ingestion by the rotor, turbulent rotor wake interaction with the stator and scattering of the turbulent eddies in the boundary layer at the trailing-edges of the rotor and the stator rows are investigated. The latter mechanism on the rotor is found to be dominant as the high rotational speed of the machine and the strong loadings induce high shear stress and pressure gradient on the blade surfaces. The global trend of the acoustic power evaluations with mass flow variation for the broadband noise levels estimated from the four contributions agree with current experimental investigations. For Strouhal numbers, based on fan diameter and tip velocity, above 3, the broadband noise spectrum is predicted within 3 dB accuracy with isolated response and free-field propagation.

INTRODUCTION

Small ventilation systems with high rotational speed are used for the cooling of avionic racks and cabin air conditioning. These compact systems of axial or mixed flow type are mainly designed by optimizing their efficiency and weight. The acoustic levels emitted by such systems are of key importance and design rules based on a long-term experience of acoustic measurements are already accounted for. Typically, the numbers of rotor blades and stator vanes are selected according to the Tyler & Sofrin criterion in order to take advantage of the duct cut-off properties and limit the emergence of the first blade passing frequencies.

In the present work, analytical aeroacoustic models that can be informed with mean flow parameters from steady-state numerical simulations are evaluated for a typical ducted axial fan system. The fan has been investigated in Safran Ventilation Systems (SVS) facilities where acoutic power has been measured in an anechoic chamber in which the duct intake is mounted. A similar facility equipped with in-duct acoustic arrays is installed at Ecole Centrale de Lyon (ECL). For the same rotational speed several mass-flow rates have been simulated which provide inputs for the acoustic prediction tool *optibrui* developped by Université de Sherbrooke. Tonal noise from the rotor-stator interaction as well as broadband noise for several noise mechanisms are investigated for 8 different mass-flow rates. Different blade response and acoustic propagation models are used to evaluate their influence in the global acoustic levels.

The present study is organised as follows. The parameters of steady-state numerical simulations are described and the performances of the fan are compared with available measurements. The main assumptions and parameters of the acoustic computations are described. Then the acoustic results are analysed first for the tonal noise mechanism, then broadband noise sources. Finally, the global acoustic spectrum is compared with available measurements.

NUMERICAL SIMULATION

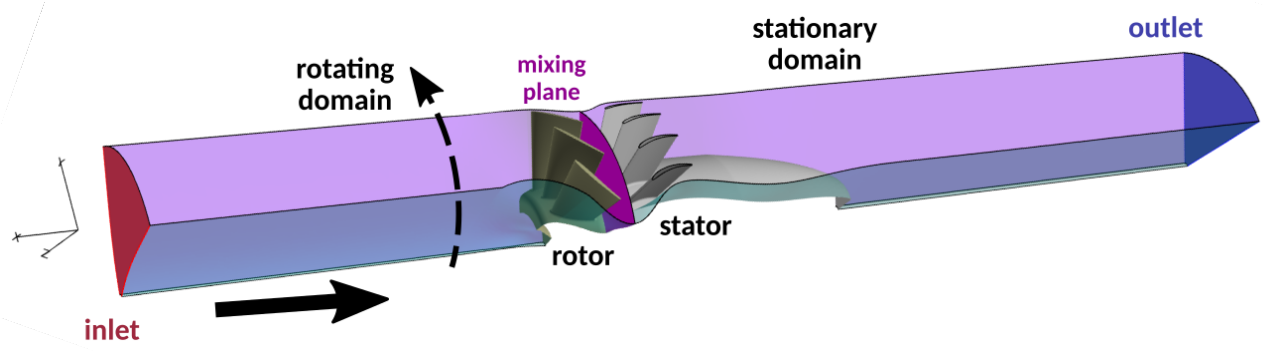

Figure 1: Overview of the computational domain.

A low-Mach number ducted axial fan from Safran Ventilation Systems is investigated in the present study. Steady Reynolds-Averaged Numerical Simulations have been performed using ANSYS CFX 17.2. The computational domain includes a long constant duct section of an angular sector of the machine containing the rotating hub, three rotor blades and four stator vanes out of the 17 and 23 total numbers respectively, and the downstream hub diffuser as shown in Fig 1. In the present simulation, the blades are considered to be identical and uniformly distributed. The stator heterogeneity due to three thickened vanes is investigated in a dedicated study [1]. An unstructured grid is created using the CentaurSoft mesher. Ten prismatic layers are set on blade and vane surfaces, while the rest of

the domain is composed of tetrahedral cells. The rotor and stator domain have about 13 million cells and 3.5 million nodes each. The maximum y^+ value is 1.4 on the rotor blades and 2 on the stator vanes ensuring a precise resolution of the boundary layers. The interface of the domains is close to the rotor trailing-edges, imposed by the short gap between the rotor and the stator rows. The mesh at mid-height of the duct in the vicinity the rotor and stator is shown in Fig. 2.

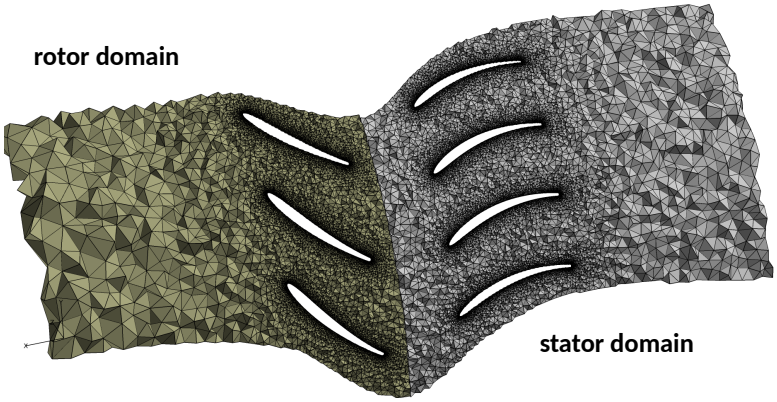

Figure 2: Crinkle view of the mesh at mid-height of the duct.

In the RANS solver, the simulation is performed using multiple reference frames and a mixing plane condition, with conservative flux transfer, is defined at the interface accounting for the pitch ratio differences between the two domains. The operating condition in the simulation is obtained by the rotation of the rotor domain, the mass inlet flow rate imposed on the inlet patch and the averaged static pressure on the outlet patch as shown in Fig. 1. Rotational periodic boundary conditions are defined for the side panels. The stationary simulations are performed using the $k-\omega$ SST two-equation model for the Reynolds stress tensor closure [2]. The simulation is converged when continuity, momentum and energy RMS residuals reach 10^{-5}, ensuring a pressure rise stabilized in the domain as well as torques on the blade and vane surfaces. For the same rotational speed, several mass-flow rates expressed in dimensionless quantities $\dot{m}^*$ have been computed around the design point ($\dot{m}^* = 1$) to evaluate the influence of the loading on the acoustic signature of the fan.

The pressure rise and the torque obtained from the simulations are shown in Fig. 3.

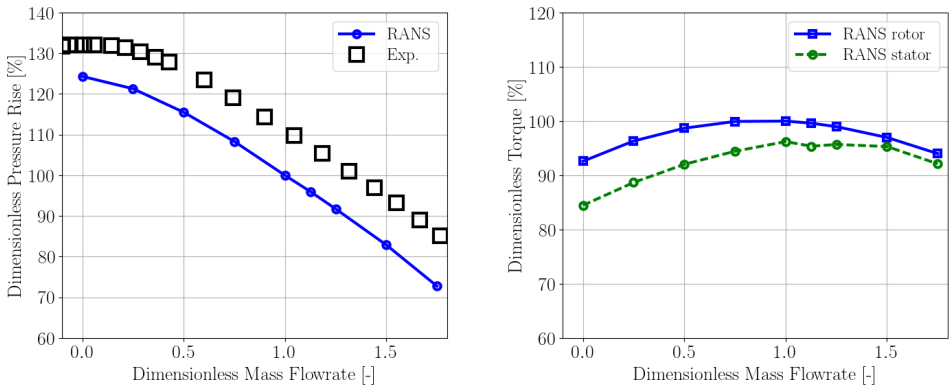

Figure 3: Pressure rise and torque obtained from the RANS simulations compared with measurements in the ECL facility.

ACOUSTICS METHODOLOGY

The tip Mach number is 0.3, and the hub-to-tip ratio is about 0.5 at the vane leading edge, limiting the number of cut-on modes in the duct section. In particular, the blade numbers have been selected to ensure that the first two blade passing frequencies (BPF) are cut-off. Nevertheless these tones appear in the acoustic spectra measured both in Safran Ventilation Systems and in the experimental installation of this fan at Ecole Centrale de Lyon [3, 1]. The tonal noise sources are investigated analytically focusing on the rotor-wake interaction on the stator vanes using the wake deficit parameters extracted from the RANS simulation. Considering the large number of vanes in the small duct diameter, the influence of cascade effects is investigated by comparing the acoustic levels obtained with an isolated airfoil response or a cascade response on this configuration. The broadband noise contributions from the rotor self-noise and the turbulent wake impingement are also estimated using isolated airfoil response and cascade response in infinite constant duct. The noise sources are modeled from statistical turbulence parameters extracted in the RANS simulation.

Strip-theory

For the implementation of analytical models, the actual blades and vanes are simplified to flat plates extruded over the radial direction. The blades and vanes are divided into 10 strip elements on which neither sweep nor lean are considered and the chord and stagger angle defined from the machine axis are assumed constant over the strip heights. This so-called strip theory allows to capture the main variations of geometry and flow parameters over the cross-section.

Acoustic propagation

For the acoustic propagation, the swirl effects are ignored. Only an inviscid mean axial flow of Mach number Ma is considered. The duct geometry for the acoustic propagation is considered as an infinite duct of constant annular duct section defined from the section at the stator row. Within these assumptions, Goldstein's analogy [4] provides the acoustic pressure in the duct. The acoustic power upstream and downstream of the machine is then computed by integrating the acoustic intensity over the duct section [5].

Regarding broadband noise, the acoustic propagation is computed from an in-duct model as previously mentionned but also from a free-field propagation model. The latter is based on the airfoil noise formulation from Amiet [6]. In both cases, the aeroacoustic model considers uncorrelated strips. For the turbulent interaction noise sources, two other models are tested that are commonly used in turbo-engine applications. Hanson's model [7] provides a cascade response with acoustic propagation in infinite unwrapped strip. It is not exactly a free-field acoustic propagation as it accounts for azimuthal mode influence, but it does not account for the duct cut-off properties. Posson's model provides a similar cascade response but accounts also for in-duct propagation.

Noise sources

For tonal noise only the rotor-wake interactions are considered as noise sources on the stator row. The excitation to be modelled is the wake deficit at the leading edge of the stator. In the RANS simulation, the rotor wakes are not convected to the stator as the mixing plane interface averages the velocity in the azimuthal direction. Two strategies are compared in the present study to estimate the excitation seen by the stator. The first approach is to assume that the wakes do not evolve and extract the velocity map just upstream the mixing plane in the rotor domain. The Fourier coefficients of the excitation are then computed from azimuthal Fourier decomposition of the upwash velocity (velocity component normal to the stator chord-line). The second approach consists in modeling the wake deficit with a

Gaussian shape, and estimating its shape parameters evolution, namely the maximum deficit and the wake width. This is done using a simple rational polynomial evolution function with distance from the rotor trailing-edge as proposed by Philbrick & Topol [8]. The rational polynomial is first adjusted from five extractions of velocity map in the rotor domain. The Fourier coefficients of the excitation are obtained by the analytical expression of a Gaussian function at the stator leading-edge.

For broadband noise, two main mechanisms are considered: the boundary-layer turbulent eddies scattering at the trailing edge of the blades and vanes (or self-noise) and the turbulent inflow impinging on the leading edge of the blades and vanes. The acoustic radiation is assumed to be uncorrelated for each strip compared with the tonal noise mechanism. The turbulence is considered as isotropic and homogeneous using a von Kármán spectra. The upwash velocity spectra is calibrated by the turbulence intensity and the most energetic turbulent wavenumber [9, 10]. The latter parameters are extracted from the RANS simulation from the turbulent kinetic energy and the turbulent dissipation frequency radial evolutions close to the leading edge of the blades and vanes. For the self noise, the excitation to be provided to Amiet's model is the wall pressure fluctuation spectra and the spanwise coherence length of the fluctuations close to the trailing-edge. The former is modelled using Rozenberg's model [11] and the latter using Salze's extension of Efimtsov's empirical model [12]. Both models rely on several boundary layer parameter definitions with the most important ones being the displacement thickness, the wall shear stress and the streamwise pressure gradient. These parameters are extracted close to rotor and stator trailing edges at several radial locations of the suction and pressure sides using an automatic procedure proposed in [13].

Performed analytical computations

The present study aims at evaluating the effect of the blade response and acoustic propagation based on the noise sources modelling described in the previous section. For the tonal mechanism, the blade response is either computed using Amiet's model [14] or using Posson's cascade response [15]. Both responses account for the in-duct propagation which prescribes the axial wavenumber and the cut-on eigen-modes for the computation of the acoustic pressure. For the broadband self-noise the blade response is computed using Amiet's model [16] with the in-duct propagation analogy or using Amiet's formulation for airfoil in free-field [6]. In the latter, the acoustic radiation for an airfoil is computed for stationary or rotating observer locations accounting for Doppler effects for a stator and a rotor respectively. For the turbulent inflow, the blade response is computed using Amiet's formulation for an airfoil in free-field [6], using Hanson's model with rectilinear cascade propagation [7] or using Posson's cascade model with infinite annular duct propagation [17]. For all investigated broadband models, the main assumption is that the acoustic contributions from individual strips are uncorrelated. To summarize the performed evaluations, the matrix is provided in Tab. 1.

Table 1: Acoustic calculations matrix.

Case	Mechanism	Excitation	Response	Propagation
RSI-iso-induct-map	TN	Velocity map	Amiet	in-duct
RSI-iso-induct-gauss	TN	Gaussian evolution	Amiet	in-duct
RSI-casc-induct-map	TN	Velocity map	Posson	in-duct
RSI-casc-induct-gauss	TN	Gaussian evolution	Posson	in-duct
BL-iso-free	BBN	Rozenberg, Salze-Efimtsov	Amiet airfoil	free-field
BL-iso-induct	BBN	Rozenberg, Salze-Efimtsov	Amiet	in-duct
TI-iso-free	BBN	von Karman	Amiet airfoil	free-field
TI-casc-free	BBN	von Karman	Hanson	cascade
TI-casc-induct	BBN	von Karman	Posson	in-duct

TONAL NOISE EVALUATION

As mentioned previously, the blade and vane numbers are selected to avoid noise emission at the first and second harmonics of the blade passing frequency in its homogeneous configuration. As the present analysis does not consider the heterogeneity of the stator row, only higher harmonics tones are obtained. For the design operating point at mass-flow rate $\dot{m}^* = 1$, the sound power levels at intake for the four analytical setups for the tonal noise (TN) mechanism are provided in Fig. 4. The differences between the isolated blade response and the cascade response are not significant on the third and fifth BPF. However, the change of wake evolution models induces differences up to 20 dB. The tone levels obtained by providing directly the velocity map before the mixing plane are higher than those obtained assuming a streamwise evolution of the Gaussian shape of the wake deficit. This highlights the critical task of defining the excitation at the leading edge of the stator from a RANS simulation.

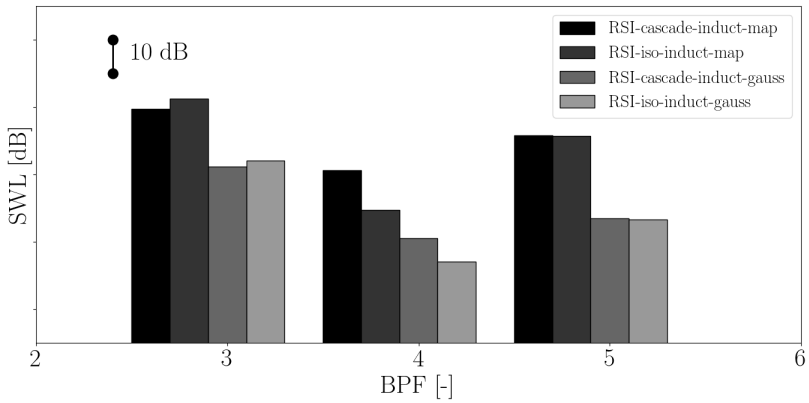

Figure 4: Tonal noise for the design operating condition computed at the intake of the machine.

For the third BPF, the tone levels as a function of mass-flow rate are provided in Fig. 5. The evolution is mainly driven by the excitation model, while the blade response induces an offset on the levels. With the velocity-map input technique, the tone level is increasing with mass-flow rate as a result of a thinner and deeper wake deficit. With the Gaussian evolution model, the results are inconsistent at low mass-flow rates where the fitting of the wake parameters provide higher excitation than with the direct velocity-map input. At high flow rates the evolution is reversed with the other excitation description. It is hard to conclude about which excitation provides the most realistic inputs and then about the variation with flow rate.

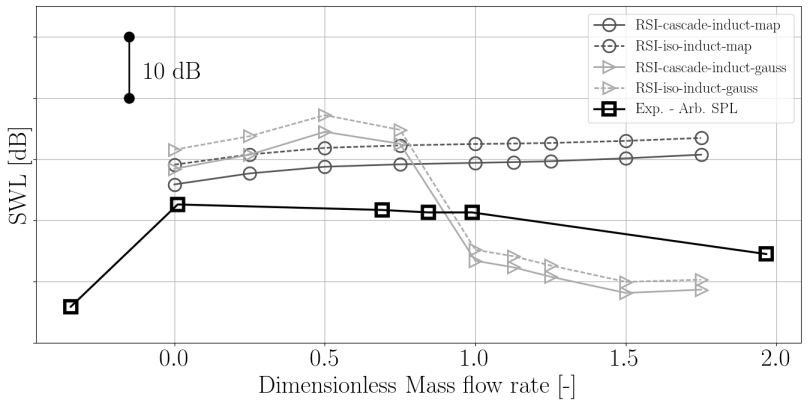

Figure 5: Third blade passing frequency tone power level at the intake of the machine.

As a first step to evaluate the evolution of the 3 BPF tone with flow rates, the experimental database acquired at ECL on the same fan in duct configuration [3] is used. In this facility, the acoustic pressure on the duct is measured with an upstream and a downstream random array of microphones. The wall pressure fluctuation spectra of the microphones from the upstream antenna are averaged together and the third BPF tone levels for the different operating conditions obtained by closing the throttle are provided in Fig. 5. These sound pressure levels (SPL) are not directly comparable in terms of levels with acoustic power (SWL), but they definitely provide an estimate of the tone evolution as a function of mass-flow rate. Therefore they are shown in arbitrary dB levels. They are in favour of a decreasing tone amplitude from the range of mass-flow rate investigated.

According to Pestana *et al.*, the third tone level is not modified by the heterogeneity [1]. High order tone levels are influenced by the quality of the wake convection and turbulent mixing. The latter could be modified by the resolution of the simulation [18, 19], the turbulent model closure, or even the presence of inlet distortions [20, 19]. Also other extrapolation techniques accounting for both viscous and potential effects could be used to evaluate the wake excitation at the stator [21] in a more physical way than the present polynomial fitting.

BROADBAND NOISE EVALUATION

For the broadband noise (BBN) modelling a total of four contributions are estimated in the present machine namely the turbulence interaction on the leading edge and the boundary-layer scattering on the trailing edge for both rotor and stator rows. The acoustic spectra obtained for the different estimations, listed in Tab. 1, are provided in Fig. 6 for the design operating condition. The frequency is made dimensionless by the fan diameter and tip rotational speed: $St = \frac{fD}{W_{tip}}$.

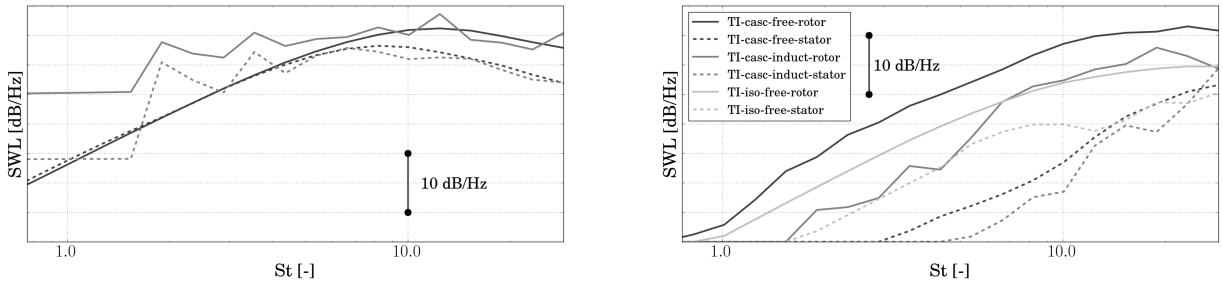

(a) Boundary layer scattering contribution.

(b) Turbulence interaction contribution.

Figure 6: Influence of the acoustic model on the broadband noise contributions at design operating condition $\dot{m}^* = 1$.

The boundary-layer scattering is similarly described with isolated blade response and free-field propagation or infinite duct propagation. The results with in-duct propagation allow capturing the cut-off influence from the duct yielding small jumps in the spectra typical of duct cut-off resonances. For the turbulence interaction contribution, larger differences appear in the results. Globally the shape of the spectral results are similar but differences up to 5 dB can be observed. Again, with in-duct propagation more irregularities are observed in the spectra caused by the duct resonances. The results obtained with the cascade response with in-duct propagation are the closest to the isolated response with free-field propagation. That confirms that cascade effects are limited in this application with a number of blades and vanes relatively low compared with a turbo-engine fan-OGV system for example. The higher levels obtained with Hanson's model are related to the particular acoustic propagation in the cascade. It could also be the consequence of the spanwise correlation model used in this par-

ticular formulation. Since this effect is not clearly understood, in the following only broadband noise contribution with isolated response and free-field contributions will be used for analyses. The use of another acoustic setup from Tab. 1 would not change the conclusions drawn latter as long as the investigation is addressung relative variations resulting from a change in parameters.

At low and high flow rates, the contributions are slightly modified resulting from the different boundary-layer development on the casing, on the blades and consequently modifying the turbulence upstream of the blades and vanes as shown in Fig. 7. The turbulent boundary-layer scattering on the rotor blades is the dominant contribution up to $St = 10$ for the low flow rate, while it is dominant over the full spectra at high flow rates. At high frequencies, the turbulent interaction on the stator leading edge is the dominant noise source for lowest flow rate, mainly resulting from the strong turbulence intensity caused by the tip vortex. The particularly high boundary layer contribution is quite surprising. It is found to be related to the strong wall shear stress τ_w and the high streamwise pressure gradient $\frac{\partial p}{\partial s}$ provided by the boundary-layer extractions. The radial evolutions of some key parameters for the boundary-layer scattering on the rotor trailing edge (the displacement thickness δ^*, the streamwise pressure gradient and the wall shear stress) are provided in Fig. 8. The quantities are made dimensionless by the tip radius R_T, the tip speed W_{tip} and the pressure rise ΔP at design condition. The dynamic pressure is hence defined as $Q_{tip} = \frac{1}{2}\rho_0 W_{tip}^2$ where ρ_0 is the reference density of the flow. The radial evolutions of some key parameters for the turbulent interaction (the turbulence intensity I, the relative velocity W and absolute velocity U on the rotor and stator leading-edge respectively) are provided in Fig. 9. The turbulence intensity is maximum at the tip due to the boundary layer developing on the casing upstream of the rotor and the tip-gap flow from the rotor upstream of the stator. The high relative velocity caused by the high rotational speed of the machine is also responsible for the high contributions from the rotor. The variation of input parameters for the excitations from low to high flow rate are smooth and do not change the main contribution ranking.

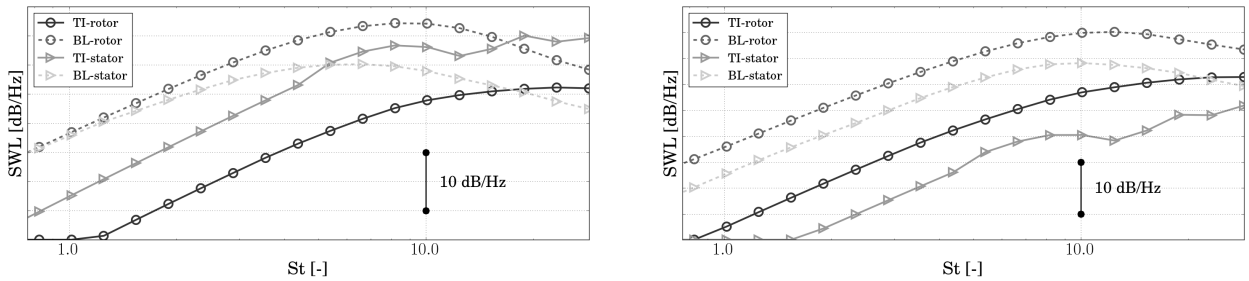

(a) $\dot{m}^*$=0. (b) $\dot{m}^*$=1.75.

Figure 7: Contributions of broadband noise sources at different mass-flow rate for isolated response with free-field propagation.

ACOUSTIC POWER SPECTRA

Broadband noise estimations using isolated response and free-field propagation, and tone estimation from isolated response and infinite duct propagation are used in this section to construct the full acoustic spectra upstream of the machine. They can be compared to acoustic power measurements performed in the SVS test facility. The acoustic sound power levels from the analytical results are integrated over the same frequency band than the experimental spectra, and the tones are spread over this same frequency band. The comparison is shown in Fig. 10. The analytical results provide a good estimation of the sound power level above a Strouhal number of 2 within 3 dB, in particular the main broadband noise level related mainly to the contribution from the boundary-layer scattering at the ro-

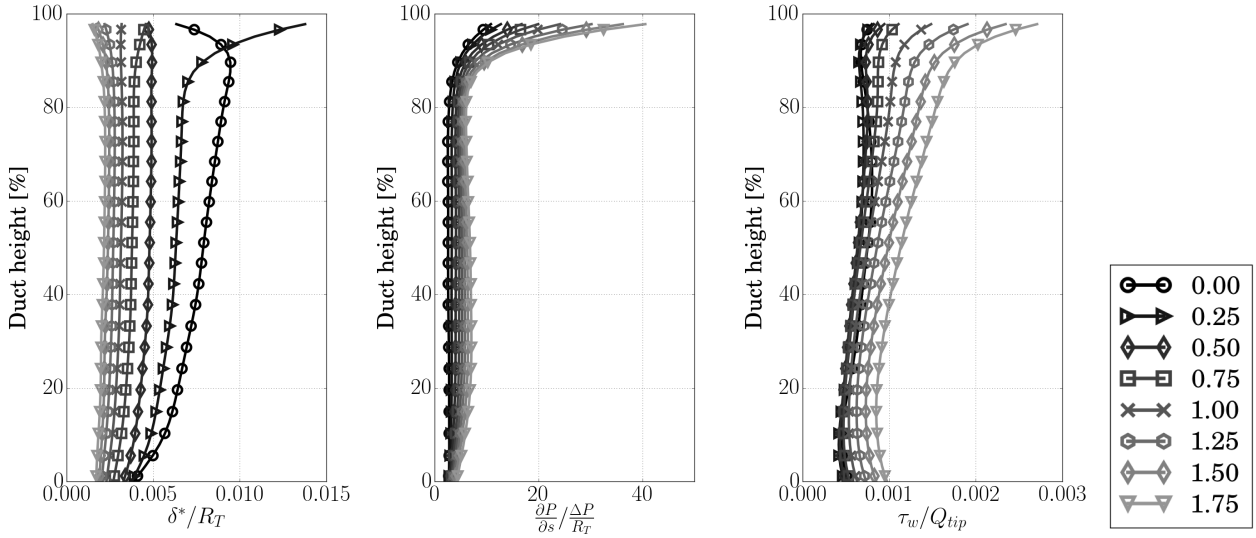

Figure 8: Boundary layer parameters upstream of the trailing edge of the rotor blade.

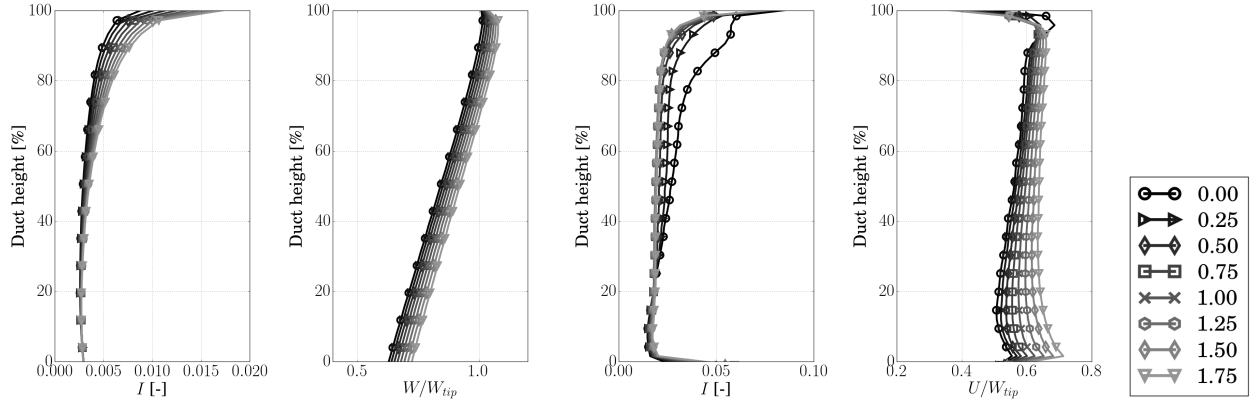

(a) Upstream of the rotor. (b) Upstream of the stator.

Figure 9: Turbulence intensity and velocity upstream of the rotor (left) and stator (right) leading edges.

tor trailing edge. The tone estimations for the third, fourth and fifth harmonics are not accurate. The lower frequency part from the experimental spectrum is related to installation effects or heterogeneity contributions that are not accounted for with the present approach. The first and second BPF tones from the experimental spectrum are related to the stator heterogeneity and are analyzed in [1].

Finally to better evaluate the ability of the present analysis to assess acoustic levels for various operating conditions, the experimental database acquired at ECL on the same fan in duct configuration [3] is used again. The averaged spectrum of all microphones of the experimental in-duct acoustic array placed downstream of the fan is shown in Fig. 11 for different operating points. The flush-mounted microphones are decontaminated from pseudo-sound according to the method presented in [22] based on the low correlation of turbulence between two different locations compared with acoustic waves.

In terms of broadband noise, the higher axial flow speed at the maximum mass-flow rate induces a higher sound pressure level. When decreasing the mass-flow rate, the broadband level tends to be lower and small differences can be observed between several operating points. However below $\dot{m}^* = 0.7$, the reduction in the flow speed inducing lower levels is compensated by highly turbulent flow occurring at the rotor and due to the high compression rate. At this condition, higher broadband levels can be measured and and the duct cut-off frequencies appear more clearly in the wall-pressure spectra due to the additional broadband modal content.

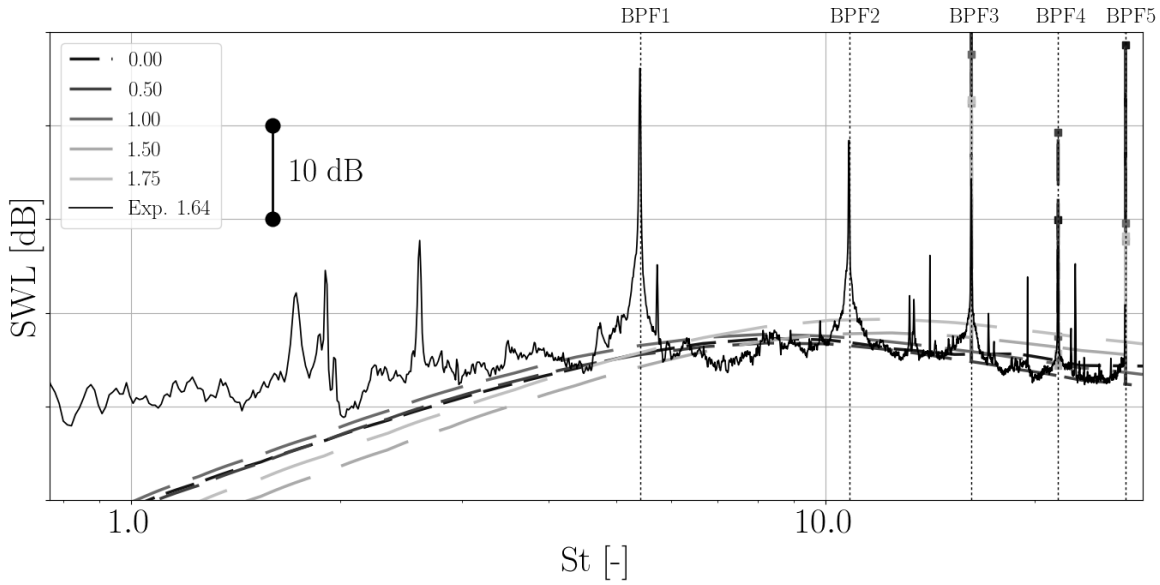

Figure 10: Sound power levels upstream of the machine. The square symbols highlight the tones for the mass-flow rate associated with the same grey colour.

In the analytical results shown in Fig. 10, the main trend of higher acoustic levels for the larger mass-flow rate is captured. At the lowest flow rate, a slight increase is also captured at high frequency. It is related to the emergence of turbulence interaction noise on the stator as identified in Fig. 7 (left). The increase is not in the same range as in the measurement, the RANS simulation may have delayed the point of stall, and cannot capture its precursory turbulent structures.

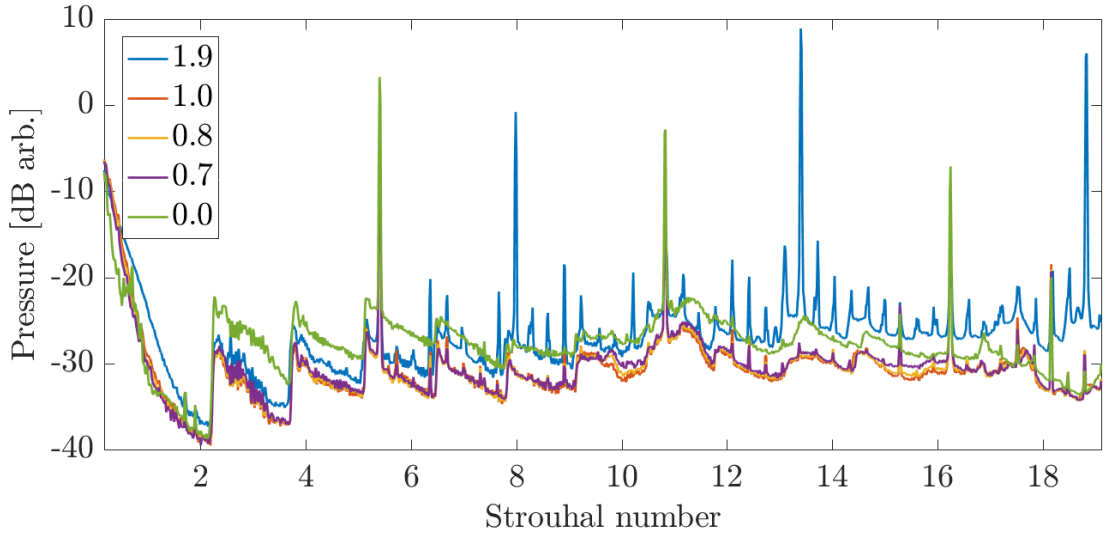

Figure 11: Sound pressure levels measured in the duct section of ECL facility.

CONCLUSIONS

A compact ducted ventilation system with high rotational speed has been investigated using RANS simulations. From the solutions at several mass-flow rates of the turbulent flow, extractions have been performed to provide inputs for a complete aeroacoustic analysis. The tonal and broadband noise mechanisms have been investigated for the homogeneous configuration of the machine. In

the aeroacoustic evaluation, several models have been further used to evaluate the influence of the blade response and the acoustic propagation. The results show that the cascade effects are limited for this configuration of hub-to-tip ratio of 0.5. The infinite duct propagation allows capturing the duct resonances but does not influence the global trend of the acoustic evaluations which are dominated by the models for the interaction mechanisms. The present investigation shows the crucial influence of the rotor wake evolution in the rotor-stator gap. The present evolution model provides good trends at high flow rates but is not robust enough for the lowest investigated flow rate. From the different broadband noise source mechanisms investigated at different flow rates the main contribution is attributed to the rotor trailing-edge noise. This peculiar behaviour compared to low-speed fan configurations is attributed to the high rotational speed of the machine and the strong loading inducing high shear stress and pressure gradient on the blade surfaces. Further investigations on the wall-pressure spectra modeling are required to further improve the confidence in the present analysis. Nevertheless the global trend with mass-flow variation of the broadband noise levels estimated from four contributions are coherent with current experimental investigations.

REFERENCES

[1] M. Pestana, M. Sanjosé, S. Moreau, M. Roger, and M. Gruber. *Investigation on the noise of an axial low Mach-number stage with a heterogeneous stator*. In *Fan 2018*, number 105, **2018**.

[2] F. R. Menter. *Two-Equation Eddy-Viscosity Turbulence Models for Engineering Applications*. AIAA J., 32(8):1598–1605, **1994**.

[3] M. Pestana, A. Pereira, E. Salze, J. Thisse, M. Sanjosé, E. Jondeau, P. Souchotte, M. Roger, S. Moreau, J. Regnard, and M. Gruber. *Aeroacoustics of an axial ducted low mach-number stage: numerical and experimental investigation*. In *23rd AIAA/CEAS Aeroacoustics Conference*, AIAA-2017-3215, **2017**.

[4] M. E. Goldstein. *Aeroacoustics*. McGraw-Hill, Inc, **1976**.

[5] R. H. Cantrell and R. W. Hart. *Interaction between Sound and Flow in Acoustic Cavities: Mass, Momentum, and Energy Considerations*. J. Am. Soc. Acoust., 36(4):697–706, **1964**.

[6] R. K. Amiet. *Noise Produced by Turbulent Flow Into a Rotor: Theory Manual for Noise Calculation*. Technical Report CR-181788, NASA, June **1989**.

[7] D. B. Hanson. *Theory for broadband noise of rotor and stator cascades with inhomogeneous inflow turbulence - including effects of lean and sweep*. Technical Report NASA/CR 2001-210762, NASA, May **2001**.

[8] D. A. Philbrick and D. A. Topol. *Development of a Fan Noise Design System Part 1: system design and source modeling*. In *15th AIAA Aeroacoustics Conference*, AIAA-93-4415, Long Beach, CA, October **1993**.

[9] S. B. Pope. *Turbulent Flows*. Cambridge University Press, **2000**.

[10] J. Christophe. *Application of Hybrid Methods to High Frequency Aeroacoustics*. PhD thesis, von Karman Institute for Fluid Dynamics / Universite Libre de Bruxelles, **2011**.

[11] Y. Rozenberg, G. Robert, and S. Moreau. *Spectral model accounting for pressure gradient and Reynolds effects for the prediction of trailing-edge noise using RANS simulations*. AIAA J., 50(10):2168–2179, **2012**.

[12] E. Salze, C. Bailly, O. Marsden, E. Jondeau, and D. Juve. *An experimental characterisation of wall pressure wavevector-frequency spectra in the presence of pressure gradients*. In *20th AIAA/CEAS Aeroacoustics Conference*, AIAA 2014-2909, Atlanta, GA, USA, **2014**.

[13] M. Sanjosé and S. Moreau. *RANS based analytical modeling of broadband noise for a low-speed fan*. In *International Symposium on Transport Phenomena and Dynamics of Rotating Machinery*, December **2017**.

[14] R. K. Amiet. *High frequency thin-airfoil theory for subsonic flow*. AIAA J., 14(8):1076–1082, **1976**.

[15] J. de Laborderie and S. Moreau. *Prediction of tonal ducted fan noise*. J. Sound Vib., 372:105–132, **2016**.

[16] R. K. Amiet. *Noise due to Turbulent Flow past a Trailing-Edge*. J. Sound Vib., 47(3):387–393, **1976**.

[17] H. Posson, M. Roger, and S. Moreau. *On a uniformly valid analytical rectilinear cascade response function*. J. Fluid Mech., 663:22–52, 11 **2010**.

[18] M. Sanjose, M. Daroukh, J. de Laborderie, S. Moreau, and A. Mann. *Tonal noise prediction and validation on the ANCF rotor-stator configuration*. Noise Control Eng. J., 63(6):552–562, December **2015**.

[19] M. Sanjosé, S. Moreau, M. Pestana, and M. Roger. *Effect of Weak Outlet-Guide-Vane Heterogeneity on Rotor–Stator Tonal Noise*. AIAA J., 55(10):3440–3457, **2017**. doi: 10.2514/1.J055525.

[20] M. Sturm, M. Sanjose, S. Moreau, and T. Carolus. *Aeroacoustic Simulation of an Axial Fan including the full test rig by using the Lattice Boltzmann Method*. In *FAN 2015, International Conference on Fan Noise, Technology and Numerical Methods*, Lyon, France, April **2015**.

[21] R. Jaron, A. Moreau, and S. Guerin. *Extrapolation of RANS flow data for improved analytical fan tone prediction*. In *21st AIAA/CEAS Aeroacoustics Conference*, AIAA Aviation, Dallas, TX, USA, jun **2015**. American Institute of Aeronautics and Astronautics. doi:10.2514/6.2015-2515.

[22] A. Finez, A. Pereira, and Q. Leclere. *Broadband mode decomposition of ducted fan noise using cross-spectral matrix denoising*. In *Fan Noise 2015*, **2015**.

ACKNOWLEDGEMENTS

The experimental database acquisition by Ecole Centrale de Lyon was performed within the framework of industrial Chair ADOPSYS co-financed by Safran Aircraft Engines and the ANR (ANR-13-CHIN-0001-01) It is also supported by the Labex CeLyA of the Université de Lyon, within the programme 'Investissements d'Avenir' (ANR-10-LABX-0060/ANR-11-IDEX-0007) operated by the French National Research Agency (ANR). The development of the acoustic prediction tool is founded by the industrial chair of Université de Sherbrooke. The numerical computations were made on the supercomputer Mammouth from Université de Sherbrooke, managed by Calcul Québec and Compute Canada.